frontiers | Frontiers in Materials

TYPE Original Research
PUBLISHED 31 July 2023
DOI 10.3389/fmats.2023.1162053

OPEN ACCESS

EDITED BY
Vladimír Šepelák,
Karlsruhe Institute of Technology (KIT), Germany

REVIEWED BY
Adewumi John Babafemi,
Stellenbosch University, South Africa
Ferhun Caner,
Universitat Politecnica de Catalunya, Spain

*CORRESPONDENCE
Hui Dou,
179204480@qq.com

RECEIVED 09 February 2023
ACCEPTED 12 July 2023
PUBLISHED 31 July 2023

CITATION
Dou H, Xu H and Xie J (2023), Long-term mechanical performance of high fluidity fiber reinforced concrete modified by metakaolin.
Front. Mater. 10:1162053.
doi: 10.3389/fmats.2023.1162053

Long-term mechanical performance of high fluidity fiber reinforced concrete modified by metakaolin

Hui Dou[1,2]*, Huaxin Xu[2] and Junjie Xie[2]

[1]School of Civil Engineering, Lanzhou Jiaotong University, Lanzhou, China, [2]Gansu Road and Bridge Construction Group Co., Ltd., Lanzhou, China

To clarify the long-term strength and toughness of metakaolin (MK) and steel fiber (SF) modified concrete with higher fluidity and water/binder ratio, a series of tests including slump tests, compression tests, splitting tests, digital image processing and Scanning Electron Microscope (SEM) tests were performed on MK-SF concrete cured for 7–360 days. Results reveal that the slump of fresh concrete decreased with an increase in the MK and SF replacement rates. Moreover, the impact of MK on the slump of steel fiber reinforced concrete (SFRC) was more pronounced when combined with a lower water/binder ratio, resulting in increased viscosity. At the pre-peak stress region of the strain-stress curve, the compressive strength f_c, tensile strength f_t, Young's modulus E_c, elastic modulus E_0, and tensile strain at peak stress $\varepsilon_{t\text{-}max}$ of high fluidity MK-SF concrete increased with increasing MK and SF admixing ratio, regardless of curing age. Notably, the coupling effects of MK and SF became more prominent after long-term curing. Without MK incorporation, the effects of SF and curing time on the above indices were relatively implicit. At the post-peak stress region of strain-stress curves, there existed a residual stage. The inclusion of MK significantly improved the long-term residual strength and strain of SFRC. Additionally, the toughness index M_c, which represents the total area of the compressive strain-stress curve containing both the pre-peak and post-peak regions, also exhibited substantial development with curing time, primarily attributed to the incorporation of MK and SF. The coupling of MK and SF led to a transformation of the concrete failure mode from brittle to ductile. Regression analysis reveals that a linear equation adequately described the long-term relationships of f_c-f_t, f_c-E_c, f_c-E_0, f_c-M_c, and f_c-$\varepsilon_{t\text{-}max}$ in MK-modified SFRC. Based on the testing data, a relative strength or toughness index λ and a new generalized hyperbola model were proposed to predict the long-term mechanical behavior mentioned above. Through crack morphology and microstructure analysis, the distinct roles of MK and SF in the composite material were examined.

KEYWORDS

geopolymer, steel fiber reinforced concrete, strength, toughness, microscopic mechanism

Highlights

- Long-term strength and toughness of high fluidity Metakaolin-Steel Fiber concrete are comprehensively investigated.
- A relative strength or toughness index and a new generalized hyperbola model are proposed to predict its long-term mechanical performance.
- By crack morphology and microstructure analysis, the different roles of Metakaolin and Steel Fiber on its long-term mechanical performance are examined.

1 Introduction

Pile foundations are commonly exposed to lateral forces caused by various factors such as wind, waves, earthquakes, dredging, and impacts. These lateral forces, in addition to the vertical forces, can affect the stability of the pile foundation. When subjected to bending moments, the stability of the pile foundation depends not only on the concrete strength before failure but also on the ductility of the concrete after cracking. In the case of driven cast-in-place piles, the concrete needs to have sufficient fluidity to ensure proper filling density. Additionally, the contraction of cast piles is significantly influenced by the resistance to deformation of high-fluidity concrete. Therefore, it is essential to consider the designed strength, toughness, fluidity, and deformation modulus in an economically efficient manner. A comprehensive consideration of various factors could ensure that the pile foundations can withstand lateral forces while maintaining structural integrity and stability.

The concrete industry produced about 1.6 billion tons of cement annually, and each 1.0 ton of cement approximately produced 0.8 ton of CO_2. Metakaolin (MK) is an effective cementing material to improve the workability of concrete and reduce the usage of cement (Siddique and Klaus, 2009; Rashad, 2013). Due to its environmental friendliness, MK has been widely used in civil engineering since the 1960s (Siddique and Klaus, 2009; Rashad, 2013). Previous studies reported that MK reduced the porosity and autogenous shrinkage, increased the hydration reaction products, and improved the durability of concrete (Poon et al., 2006; Siddique and Klaus, 2009; Güneyisi et al., 2010; Melo and Carneiro, 2010; Kou et al., 2011; Megat Johari et al., 2011; Antoni et al., 2012; Bernal et al., 2012; Güneyisi et al., 2012; Madandoust and Mousavi, 2012; Ramezanianpour and Bahrami Jovein, 2012; Duan et al., 2013; Rashad, 2013; Han et al., 2018). The pozzolanic activity of blast furnace slag or lime was effectively excited by MK (Bernal et al., 2012; Güneyisi et al., 2012; Duan et al., 2013). While, the fluidity of concrete significantly reduced with MK addition, and thus a larger amount of high-efficiency water-reducing agents are need (Megat Johari et al., 2011; Madandoust and Mousavi, 2012; Rashad, 2013). Indicated that the strength of concrete decreased with excessive replacement rate of MK (Poon et al., 2006). Recently, Akcay and Tasdemir pointed out that the brittleness of concrete increased with the addition of MK (Akcay and Tasdemir, 2018). In addition, the addition of steel fiber (SF) not only improved the compressive strength of concrete (Qiana and Stroeven, 2000; Yao et al., 2003; Song and Hwang, 2004; Yazıcı et al., 2007; Mohammadi et al., 2008; Holschemacher et al., 2010) but also changed the brittle failure of concrete to ductile failure (Holschemacher et al., 2010). While, the excessive addition of SF could reduce the slump of concrete (Yazıcı et al., 2007; Mohammadi et al., 2008; Güneyisi et al., 2014; Akcay and Tasdemir, 2018).

Many studies investigated the performance of steel fiber and MK incorporation on the mechanical properties of concrete. Investigated the effectiveness of MK and two types of steel fiber with different length/aspect ratios on the compressive, flexural, splitting, and bonding strength of the concretes at a water/binder ratio (w/b) of 0.35 (Güneyisi et al., 2014). Clarified the performance of Roller Compacted Concrete Pavement modified by using MK and shredded recycled steel fibers (SRSF). The results in terms of specific gravity, ultrasonic pulse velocity, compressive strengths, and split tensile strengths at 28 days showed that the effect of SRSF was dependent on other components of the mixture, especially the MK (Noroozi et al., 2019). Investigated the bonding strength of MK-based geopolymer concrete reinforced by steel and glass fiber (Albidah et al., 2020). Mehdipour et al. (2020) focused on the mechanical properties and durability of rubberized concrete combined with steel fiber and MK at w/b of 0.45 and high temperatures. Studied the roughness of microstructural faces of MK concrete based on AFM tests (Yu et al., 2022).

It is well-known that compressive strength and elasticity modulus are the main mechanical properties of concrete (Del Savio et al., 2022). Numerous researchers have established the correlation between compressive strength and other mechanical indices based on statistical analysis (Kim et al., 2022). Mahapatra and Barai performed compression tests, split tests, bending tension tests, ultrasounds, and sclerometers to evidence the correlation between compressive strength and modulus (Mahapatra and Barai, 2019). Proposed a strength prediction model with a 0.94 correlation coefficient based on an analysis of ultrasonic pulse velocity (Shafigh et al., 2016). Showed a variation of splitting tensile strength with compressive strength for geopolymer concrete subjected to different heat curing or ambient curing (Mohammed et al., 2021). The relationships between splitting tensile strength, compressive strength, flexural strength, and elastic modulus, and several prediction equations were obtained from regression analysis. Proposed a unified empirical model to describe the multiaxial compressive strength of hybrid fiber-reinforced concrete (Li et al., 2023). However, the analysis of the correlation between long-term strength, deformation modulus, and toughness of MK-modified fiber-reinforced concrete is still lacking.

Despite numerous studies conducted on MK-modified concrete over the past few decades, there are still several unresolved issues: 1) The coupling effects of adding MK and SF on the long-term mechanical performance of high fluidity concrete, such as strength, ductility, and deformation modulus, are not yet fully understood. 2) There is a lack of quantitative prediction models for the development of strength and toughness in MK-modified concrete at different curing ages. 3) The crack development and microstructure of steel fiber reinforced concrete (SFRC) with MK incorporation after long-term curing have not been reported. These unresolved issues highlight the need for further research in order to fully understand the potential of MK-modified concrete and its combination with SF for various applications.

To address the shortcomings mentioned earlier, a comprehensive experimental study was conducted. Various tests,

10.3389/fmats.2023.1162053

including slump tests, compression tests, splitting tests, and digital image processing, were performed on MK-SF concrete samples at different curing durations of 7, 28, 60, 90, 180, and 360 days. Additionally, Scanning Electron Microscope (SEM) tests were conducted to examine the microstructure of the concrete. The mechanical performance of the high fluidity MK-SF concrete, including compressive strength, tensile strength, Young's modulus, elastic modulus, total absorb energy until failure and tensile strain at peak stress, was thoroughly investigated based on the results obtained from these tests over an extended period. A new generalized hyperbola model was proposed to predict the long-term mechanical behavior of the MK-SF concrete. Moreover, by analyzing the crack morphology and microstructure of the concrete using SEM, the different roles of MK and SF in the mechanical performance of high-fluidity concrete were examined.

Overall, this study aimed to address the knowledge gaps and contribute to a better understanding of the long-term mechanical behavior and microstructure of MK-SF concrete in a high fluidity state. The findings from this research would help in optimizing the design and application of MK-SF concrete in various construction projects.

2 Materials and methods

2.1 Materials

The specific surface area of selected Ordinary Portland Cement (OPC) is 348 m^2/kg. The MK agents used in this study are produced by BASF Company, Germany. The chemical components and proportion in the mass of the OPC and MK were determined by X-Ray Fluorescence (XRF) method and listed in Table 1. The particle size distributions of raw materials based on sieving tests and Laser Particle Size Analyzer tests are shown in Figure 1. The coarse aggregate used is limestone with a minimum size of 4.75 mm. The fine aggregates are mainly quartz sand and the fine parts (smaller than 0.075 mm) are less than 6%. A milled steel fiber with a 2.5 mm width and 35 mm length was selected. The morphological characteristics of raw materials were summarized in Table 2. The polycarboxylic acid solution was selected as the High Range Water Reducing Agent (HRWRA). Based on reported X-Ray Diffraction (XRD) patterns (Yu et al., 2022), there are no apparent peaks in XRD pattern of MK. The OPC is mainly composed of C3S, C2S, C3A, C4AF, Calcite, and Gypsum.

2.2 Sample preparation

All samples were prepared following the Chinese standard GB/T 50081, and cured in a cubic mold with 100 mm side length. After 7, 28, 60, 90, 180, and 360 days, the compressive strength and split tensile strength were determined. As shown in Table 3, the MK15-SF3 represents that the mass ratio of MK to OPC is 15%, and the mass content of SF is 3% as part of the cemented material (OPC and MK). Since then, the identities of other experimental groups represent the same meanings as above. The mixing proportions of aggregates, water, and HRWRA in concrete are also listed in Table 3. The w/b ratio used for determining mechanical properties is 0.6.

TABLE 1 Chemical composition of OPC and MK (w_t%).

Oxides (%)	OPC	MK
Al_2O_3	4.92	33.62
SiO_2	14.34	62.68
K_2O	0.62	0.18
CaO	52.84	0.07
Na_2O	0.33	0.19
MgO	1.58	—
Fe_2O_3	3.05	0.41
$*CO_3$	20.54	1.69
LOI	1.78	1.16

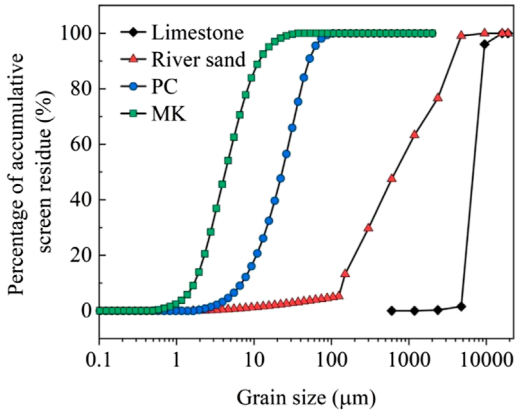

FIGURE 1
Cumulative particle size distribution of sand and gravel.

TABLE 2 Morphological characteristics of selected materials.

Raw materials	Property
Limestone gravel	The max particle size ≤ 15 mm
River sand	Uneven yellow particles and the max particle size ≤ 5 mm
Milled steel fibers	The shape is wavy, the length is 35 mm, the width is 2.5 mm, the thickness is 1 mm
Metakaolin	Uniform white powder and the max particle size ≤ 31.11 μm
Portland cement	Uniform grey powder and the max particle size ≤ 89.99 μm

The OPC, MK, SF, and aggregates were firstly mixed in a dry state, and then the HRWRA solution and water were added. The mixing time was 3 min at least, and the mixtures in the mold were vibrated within 15 min. After 24 h of curing in a standard curing cabinet with a temperature controller error of 20°C ± 2°C, the specimens were de-molded and placed in a standard environment again (temperature of

TABLE 3 Proportions of MK-SF concrete.

Sample ID	OPC [kg/m Antoni et al. (2012)]	MK [kg/m (Antoni et al. (2012)]	SF [kg/m (Antoni et al. (2012)]	Fine aggregates [kg/m (Antoni et al. (2012)]	Coarse aggregates [kg/m (Antoni et al. (2012)]	Water [kg/m (Antoni et al. (2012)]	HRWRA [kg/m (Antoni et al. (2012)]	w/b
MK0-SF0	426.0	0	0	720.0	1080.0	255.6	1.278	0.6
MK15-SF0	362.0	64.0	0	720.0	1080.0	255.6	1.278	0.6
MK10-SF0	383.0	43.0	0	720.0	1080.0	255.6	1.278	0.6
MK0-SF2	426.0	0	8.52	720.0	1080.0	255.6	1.278	0.6
MK15-SF2	362.0	64.0	8.52	720.0	1080.0	255.6	1.278	0.6
MK10-SF2	383.0	43.0	8.52	720.0	1080.0	255.6	1.278	0.6
MK0-SF3	426.0	0	12.78	720.0	1080.0	255.6	1.278	0.6
MK15-SF3	362.0	64.0	12.78	720.0	1080.0	255.6	1.278	0.6
MK10-SF3	383.0	43.0	12.78	720.0	1080.0	255.6	1.278	0.6

20°C ± 2°C, relative humidity greater than 95%) for different curing durations.

2.3 Experimental set-up

2.3.1 Slump tests

According to the Chinese standard GB/T 50080-2016, the slump of concrete was measured using a standard bell-shaped bucket. This bucket has an upper opening with a diameter of 100 mm, a bottom opening with a diameter of 200 mm, and a height of 300 mm. During the slump test, a volume of concrete equal to 2.5 times the volume of the standard slump bucket was mixed each time. This ensures that there is enough concrete to fill the bucket completely. Each group of tests was conducted twice to ensure accuracy and consistency. The recorded slump value is the average of the two samples tested. To prevent moisture loss and maintain the workability of the concrete, the samples were covered with plastic film during the tests. This helps to prevent the evaporation of water from the concrete surface. It is also important to note that each group of tests should be completed within 15 min. This time restriction helps to ensure that the concrete does not undergo significant changes in workability before the slump test is conducted.

2.3.2 Compression and tensile strengths

According to the Chinese standard GB/T 50081-2002, an MTS (Mechanical Testing System) hydraulic servo universal testing machine with a capacity of 2,000 kN was used to conduct compressive strength and split tensile strength tests. The schematic diagrams of the test setup were shown in Figures 2A, B. These diagrams provide visual representations of how the samples were positioned and loaded during the tests. The loading rate for both compressive and split tensile strength tests was 0.5 mm/min. During the tests, data recording was done at a frequency of 1/10 s. This high frequency of data recording ensures that accurate and detailed information about the behavior of the concrete under load is captured. To determine the compressive strengths and tensile strengths, three parallel samples were tested for each group. The average value of these three samples was taken as the representative compressive strength or tensile strength for that group. Furthermore, the destruction processes of the samples were recorded using digital images to visually document the behavior of the concrete as it progressed toward failure.

2.3.3 Young's and elastic modulus

The Young's modulus and elastic modulus were calculated by analyzing the unconfined compressive and tensile stress and strain curves. Following American standard ASTM E111, the Young's modulus E_c (Eq. 1) is defined as the secant slope between contact stress σ_c, 1.0 MPa, and inflexion stress σ_f of linear increase and sharp increase of strain.

$$E_c = \frac{\sigma_f - \sigma_c}{\varepsilon_f - \varepsilon_c} \quad (1)$$

Where ε_c and ε_f are strains that correspond to contact stress σ_c and inflexion stress σ_f.

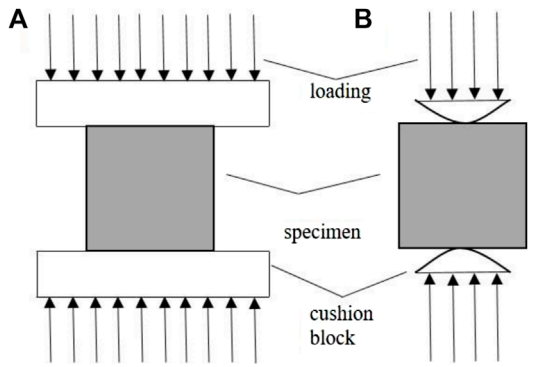

FIGURE 2
Schematic diagram of test set-up: **(A)** Compression test; **(B)** Split tension test.

The elastic modulus E_0 was calculated based on the stress-strain curves of MK-SF concrete before their cracking in splitting tensile tests.

$$E_0 = \frac{\sigma_{t-max}}{\varepsilon_{t-max}} \quad (2)$$

Where E_0 is the represented elastic modulus of MK-SF concrete, $\sigma_{t\text{-}max}$ is the splitting tensile strength, and $\varepsilon_{t\text{-}max}$ is the strain corresponding to maximum splitting tensile stress.

2.3.4 SEM

Following the compression tests, the concrete samples were analyzed using a JSM-5600LV low-vacuum scanning electron microscope (SEM) with a resolution of 3.5 nm. The SEM images allowed for the observation of the microstructures of the hydrated cement, as well as the bonding and cracks between the hydration products and the aggregate. The images were captured at a magnification of 2,000 times, providing a detailed view of the concrete's internal structure.

3 Results

3.1 Slump

In previous studies, the mechanical behavior of MK concrete has drawn more attention. While, the slump, a key parameter for evaluating the liquidity of concrete, was less considered in the application of pumping piles (Güneyisi et al., 2010; Antoni et al., 2012; Bernal et al., 2012; Güneyisi et al., 2012; Duan et al., 2013; Han et al., 2018). The slump of samples with different ratios of water to binders, including OPC and MK, at w/b = 0.3, 0.4, and 0.6, are shown in Figure 3. Generally, the slump of fresh concrete decreased with an increase in the MK replacement rates or SF content. For example, when SF = 0%, w/b = 0.6, and MK was increased from 0% to 15%, the slump decreased from ~200 mm to ~170 mm. Meanwhile, it decreased from ~200 mm to ~170 mm as MK = 0, w/b = 0.6, and SF increased from 0% to 3%. It is interesting that the slump of MK-SF concrete was within 160–170 mm when MK was incorporated and w/b = 0.6, indicating that the influence of MK on the reduction of fluidity is more pronounced in these conditions.

In the case of MK-treated fresh concrete with a higher water-to-binder ratio (w/b), it exhibited a high fluidity value with a slump ranging from 160 mm to 200 mm. This meets the basic requirements for pumping concrete. However, as the w/b ratio decreased, the slump decreased to approximately 100 mm. On the other hand, regardless of the presence of MK, the slump of SF-reinforced concrete significantly decreased as the SF content increased. However, when the MK content was higher, the addition of SF had almost no influence on the fluidity of the concrete. For instance, when the MK content is 15% and the SF content ranges from 0% to 3% at w/b ratios of 0.3 and 0.4, only a slight reduction of around 10 mm in slump is observed.

These findings suggest that the combined influence of SF and MK on the fluidity of fresh concrete is not significant when the MK content is higher. The lowest slump observed in fresh concrete, at a w/b ratio of 0.6, is approximately 160 mm, which still meets the basic requirements for pumping concrete. However, it is worth noting that the addition of SF and MK does lead to a reduction in fluidity and can affect the workability of the concrete mixture. Therefore, even though a w/b ratio of 0.3 and 0.4 are recommended for their higher mechanical performance, it is important to consider the impact on fluidity and workability when incorporating SF and MK.

3.2 Compressive and tensile strengths

Over the past several decades, many researchers investigated the influence of curing time on the compressive strength development of normal concrete. However, little experimental data considering the long-term strength development of high fluidity MK-SF concrete is reported. The compressive and tensile strength development of MK-modified concrete with a w/b ratio of 0.6 after 7–360 days of curing is shown in Figure 4. The coefficients of variation for the strength of MK-SF concrete at different curing age ranges from 0.04 to 0.13, and the mean value is 0.08.

According to Figure 4A, the compressive strength of the concrete increased with an increase in the replacement rate of MK at different curing stages, while keeping the amount of SF constant. Comparing the long-term strength (at 360 days) to the standard compressive strength (at 28 days), it is observed that without any MK incorporation, the long-term strength was approximately 1.04–1.14 times higher. However, when MK was added, the long-term strength increased even further to approximately 1.18–1.41 times higher. In the group where SF content was 0%, the compressive strength remained stable after 90 days of curing. However, in the groups where SF content was 2%–3% and MK content was 10%–15%, the compressive strength continued to increase beyond 90 days of curing.

In the early stage, the compressive strength of the concrete with MK15-SF0 was approximately 1.62 times higher than that with MK0-SF0. When the MK substitution rate was 0%, the compressive strength was improved by approximately 1.4 times by adding 3% SF. On the other hand, the compressive strength of MK10-SF3 was approximately 1.10 times higher than that of MK10-SF0. As the curing period progressed, the addition of MK improved the hydration reaction and enhanced the interface between SF and

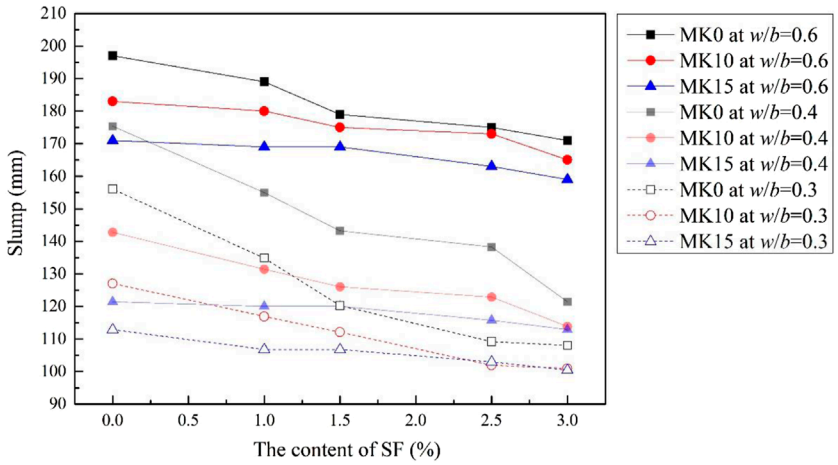

FIGURE 3
Slump of MK-SF concretes with different w/b ratio.

the hydration product. After a curing period of 360 days, the compressive strength of MK15-SF3 reached 51.3 MPa, while that of MK0-SF0 was 26.5 MPa. This indicates that the coupled effects of MK and SF become more evident after long-term curing.

Previous studies showed that MK significantly reduced the internal defects in concrete, and SF restricted the relative movement of various components after cracking (Güneyisi et al., 2014; Han et al., 2018). In this study, it is confirmed that the compressive strength f_c of high fluidity concrete increased with the increase of MK and SF. After 360 days of curing, the compressive strength of MK0-SF0 was 26.5 MPa, MK0-SF3 was 29.2 MPa, and MK15-SF0 was 36.0 MPa. The long-term strength of MK15-SF0 was significantly higher than that of MK0-SF3, indicating that MK played a more important role in improving compressive strength. When MK increased to 15% and SF increased to 3%, the combined improvement of SF and MK on compressive strength reached 1.41 times. This suggests that the combination of SF and MK has a synergistic effect on enhancing the compressive strength of the concrete.

Figure 4B presents the results of splitting tensile tests conducted on MK-SF concrete with a water-to-binder ratio of 0.6 at different curing periods. When the amount of SF was kept constant, the tensile strength of MK-SF concrete increased with an increase in the MK mixing rate, particularly in the early stage of curing. This trend continued in the long term, with the gap between different MK mixing rates becoming more significant. Regardless of the SF content, the tensile strength of MK15-SF0 was 2.76 times higher than that of MK0-SF0 after 7 days of curing, and 3.1 times higher after 360 days of curing. For SF content of 3% and MK content of 15%, the tensile strength (f_t) ranged from 6.9 to 11.2 MPa from 7 to 360 days of curing. While, MK0-SF3 exhibited a lower tensile strength, ranging from 2.99 to 3.41 MPa, and this variation was dependent on the curing period. It is observed that without the incorporation of MK, the effect of curing time on the tensile strength was not significant. Based on these results, it is concluded that MK is the key factor controlling the long-term tensile strength of high-fluidity MK-SF concrete. The SF content does not contribute significantly to the tensile strength without the presence of MK in the mix.

3.3 Stress-strain behavior

Figure 5 in the study shows typical compressive and tensile stress-strain curves of MK-SF concretes with a water-to-binder ratio of 0.6 after 7, 28, and 360 days of curing. Without SF, the maximum compressive and tensile stress, as well as the yielding strain, increased with an increase in the MK content. For MK-modified concrete, the strain corresponding to the compressive and tensile strength reached values of 0.005–0.01 and 0.003–0.005, respectively. On the other side, the corresponding values for normal concrete were approximately 0.002–0.0033 and 0.0001, respectively. Over time and with increasing MK content, three important characteristics of the compressive stress-strain curve increased, referring to maximum compressive stress, secant slope before yielding, and residual stress after failure. These characteristics of the tensile stress-strain curve also increased with curing time and MK content. Notably, the long-term tensile strain of MK-modified concrete without SF, corresponding to the maximum stress, decreased with increasing curing time, indicating that the long-term brittleness increased when MK was incorporated into the mix. With the presence of SF, both the failure strain and residual stress after failure at both the long-term and early stages increased compared to the group without MK. This suggests that the addition of SF enhances the ductility and resistance to cracking in MK-SF concrete. These findings demonstrate the influence of MK and SF on the mechanical behavior and performance of concrete, with MK affecting the long-term brittleness and SF enhancing the ductility and crack resistance of the material.

The analysis of Figures 5A, B shows that the maximum strengths of MK0-SF0, with no MK or SF added, cured for 7, 28, and 360 days, corresponding to a similar compressive strain of 1.0%. However, by adding MK, the yielding strain increases to 1.2%–1.3%

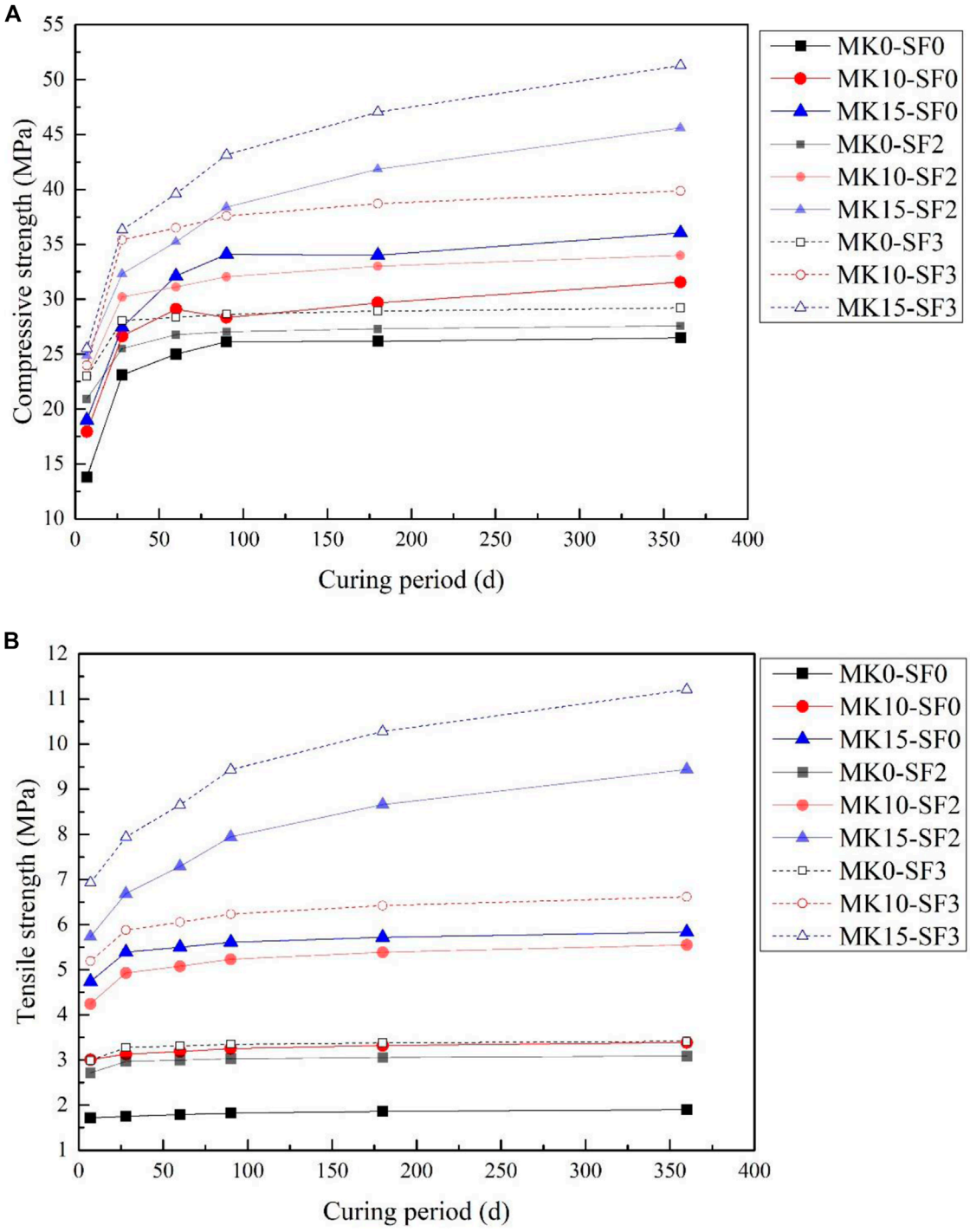

FIGURE 4
Strengths of MK-SF concretes with different curing times: **(A)** Compressive strengths **(B)** Splitting tensile strengths.

with increasing curing time. The results shown in Figures 5C, D indicate that SF incorporation provides higher residual stress and the ultimate strain after failure increases. At the yielding to failure stage, the residual stresses after failure in MK0-SF3, MK10-SF3, and MK15-SF3 concretes, which corresponds to approximately 10–15 MPa, were 2–3 times higher than in MK concrete without SF. Furthermore, when comparing the long-term compression strength of MK0-SF0 with MK15-SF0, it is observed that it increased from 25 MPa to 45 MPa with the addition of MK. Additionally, the compression strengths of MK15-SF0 and MK15-SF3 after 360 days of curing are close to 45 MPa. This indicates that SF primarily enhances the residual compressive strength of the concrete after cracking, rather than increasing the maximum strength before cracking occurs.

10.3389/fmats.2023.1162053

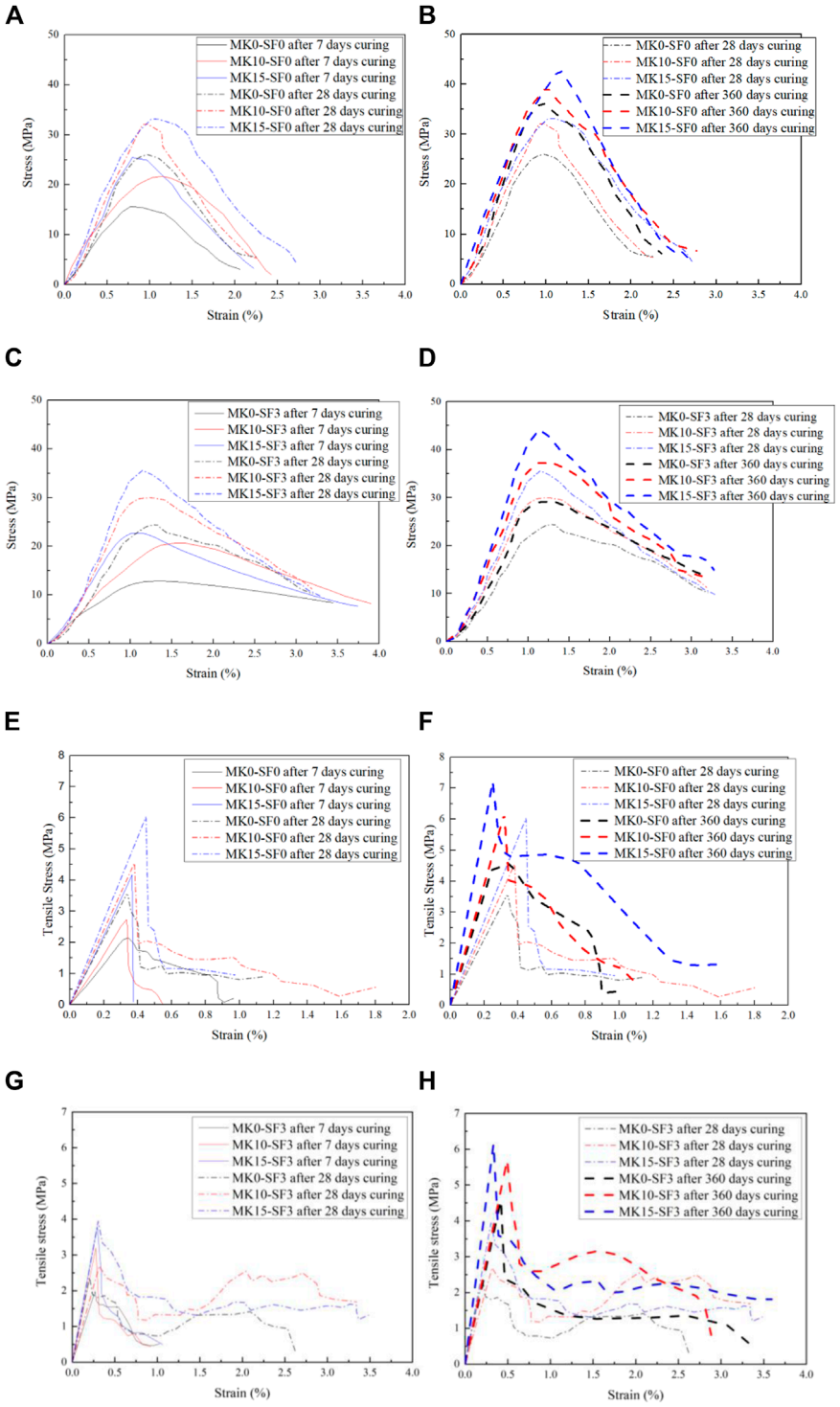

FIGURE 5
Stress versus strain of MK-SF concretes: **(A–D)** compressive stress-strain curves of MK group and MK-SF group after 7, 28, and 360 days; **(E–H)** tensile stress-strain curves of MK group and MK-SF group after 7, 28, and 360 days.

In Figures 5E, F, it is observed that MK-modified concrete without SF exhibited a brittle failure mode under tensile loading. The tensile stress and strain linearly increased initially, but the MK concrete suddenly broke instead of deforming further. However, with increasing curing time, the addition of MK significantly improved the tensile strength of the concrete. For MK0-SF0, the tensile strengths were 2.0, 3.5, and 3.5 MPa at 7, 28, and 360 days, respectively. On the other hand, for MK15-SF0, the tensile strengths are 4.1, 6.0, and 7.0 MPa at 7, 28, and 360 days, indicating a significant improvement during the period of 28–360 days due to the addition of MK. Interestingly, after long-term curing, MK15-SF0 suddenly failed at a smaller tensile strain, while a residual stress of

10.3389/fmats.2023.1162053

1.5 MPa is still present. Figures 5G, H demonstrate that the addition of SF significantly changed the brittle failure mode of the concrete to a more ductile failure mode. The ultimate tensile failure strain of MK-SF concrete reached 1.0% at the early stage and eventually reached 2.5%–3.0% with time. Unlike the concrete without SF, the SF-treated samples, especially those with MK incorporation, did not completely destruct after reaching the maximum tensile stress. While the addition of SF and MK individually improves the tensile strengths of the concrete, the coupling effects of them are not evident at the early stage. For example, the difference in tensile strength between MK15-SF0 and MK15-SF3 is within 0.5 MPa after 7 days of curing. Similarly, the residual tensile strengths of MK0-SF3 and MK15-SF3 are close after 7 days of curing, being around 0.5 MPa. However, with increasing curing time, the coupling effects of SF and MK on residual tensile stress and strain become more evident.

3.4 Young's and elastic modulus

According to ASTM E111, the Young's modulus (E_c) of MK-SF concrete is determined by analyzing the unconfined compressive stress and strain curves. It is calculated as the secant slope between the contact stress of 1.0 MPa and the inflection stress where the linear increase in strain transitions to a sharp increase. This modulus represents the material's ability to withstand changes in length when under lengthwise compression. On the other hand, the elastic modulus (E_0) of MK-SF concrete is defined as the slope from the initial point to the peak point in the curve of tensile stress and strain. Both the Young's modulus (E_c) and the elastic modulus (E_0) provide an indication of the resistance to deformation of MK-SF concrete before the development of cracks. As shown in Figure 6, Young's modulus of MK-SF concrete (w/b = 0.6), which is based on elastoplastic strain, and its elastic modulus, which is based on elastic strain, significantly increased with an increase in the MK and SF replacement rate. The coupling effects of MK and SF are more prominent after long-term curing.

In Figure 6A, the results show that the addition of MK increased the Young's modulus of the concrete from 7 days to 360 days, without the addition of SF. The increase in Young's modulus ranged from 1.57 to 1.67 GPa; for normal concrete, cement hydration products increased by 1.31 GPa over the curing period. When SF was added at 2% and 3%, the inclusion of 10% MK in the concrete led to a 1.12 and 1.25 fold increase, respectively, compared to the MK0-SF2 mix after long-term curing. Similarly, for MK15-SF2 and MK15-SF3 mixes, the Young's modulus was 1.29 and 1.89 times higher, respectively, compared to the MK0-SF3 mix after 360 days of curing. This suggests that MK enhanced the interface between the hydration matrix and SF after extended curing periods. However, at the early stage, the Young's modulus of MK-SF concrete was relatively similar regardless of the replacement rate.

The results shown in Figure 6B demonstrate the change in the elastic deformation resistance property of MK-SF concrete over time. The elastic modulus increased with an increase in the replacement rate of MK and SF at different stages of curing. When 15% MK was added without SF, the elastic modulus (E_0) was

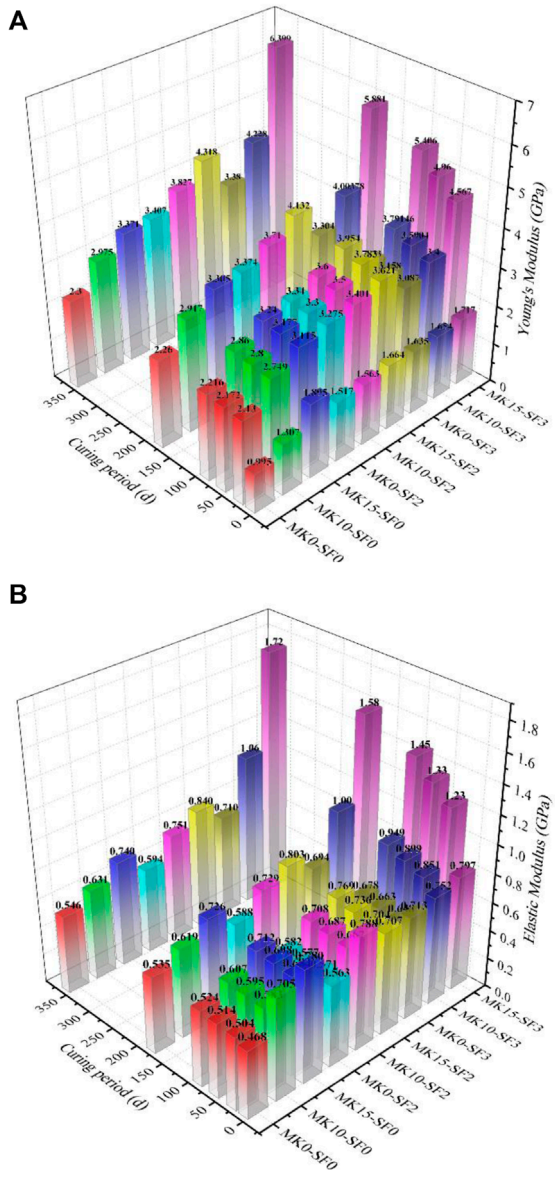

FIGURE 6
The Young's and elastic modulus of MK-SF concretes changed with curing time: **(A)** Young's modulus; **(B)** elastic modulus.

0.2 GPa higher compared to the MK0-SF0 mix. For the cement-based composite MK0-SF0, the increase in elastic modulus due to cement hydration products was only 0.1 GPa with an increasing curing period. When SF was added at 3%, the inclusion of 15% MK led to a significant increase of 1.41 and 2.16 fold in elastic modulus for long-term curing. Possibly, the SF restrained the movement of the hydration matrix, while MK promoted cohesive strength after extended curing periods. At the early stage, the elastic modulus of MK-SF concrete ranged from 0.47 to 0.80 GPa, regardless of the replacement rate. Then, the coupling effects of MK and SF on the increase in elastic modulus were not evident after 7 days of curing. However, the long-term behavior of MK-SF concrete was prominently influenced by the coupling effects between these two elements.

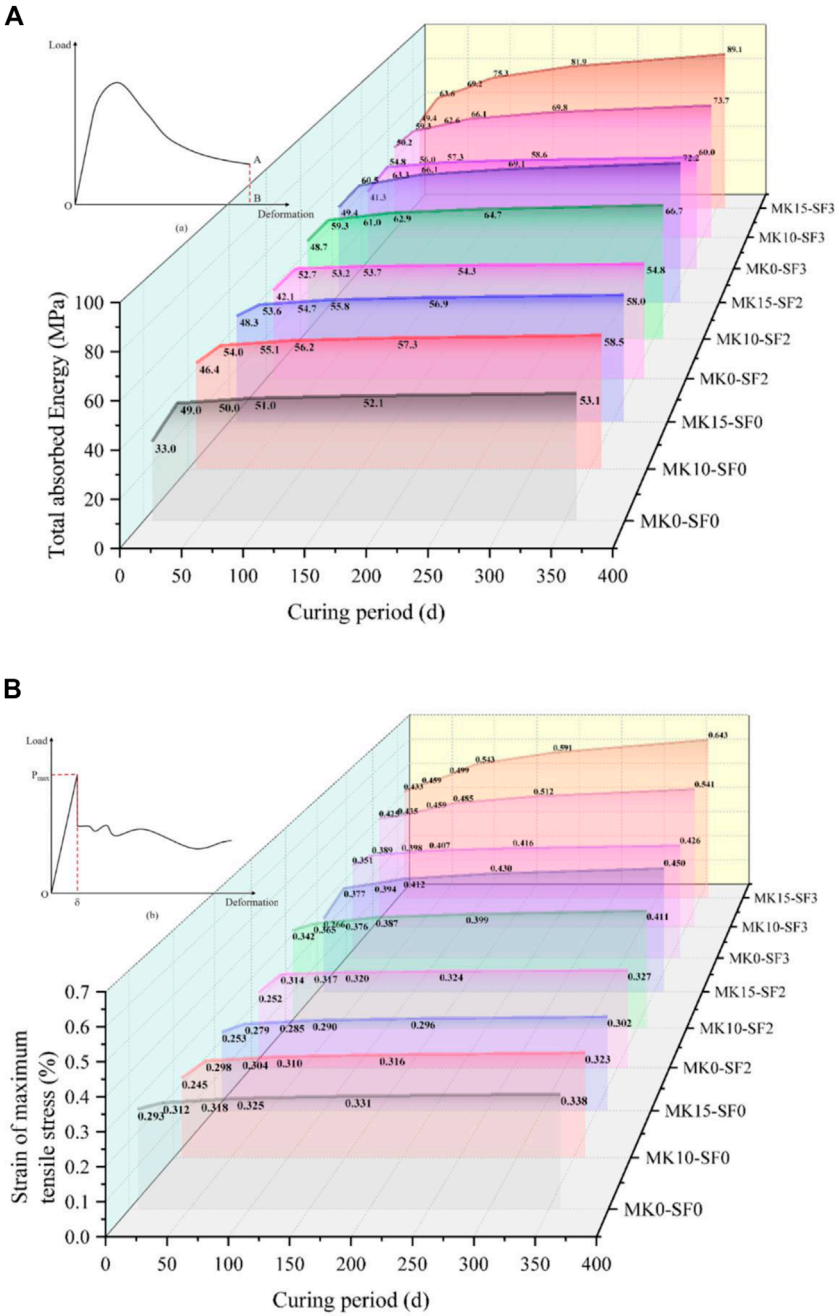

FIGURE 7
Long-term toughness of MK-SF concrete: **(A)** total adsorbed energy; **(B)** failure strain corresponding to maximum tensile stress.

4 Discussions

4.1 Long-term toughness

Toughness is the ability of a material to absorb energy and plastically deform with or without fracturing. In this paper, one definition of toughness is the area under the entire compressive strain-stress curve (Figure 7A). Another definition of toughness, or ductility, is determined from the failure strain in the post-peak region (Figure 7B). For a material to be considered tough, it must possess both strength and ductility. The typical stress-strain curves of a ductile material and a brittle material are shown in Figure 5. For example, brittle materials like MK15-SF0 cured for 7 days that are suddenly destroyed but with limited ductility are not tough. Conversely, very ductile materials such as MK15-SF3 cured for 7 days with low strength are also not tough. Thus, an ideal material should withstand both high stresses and high strains in order to be tough. Toughness is related to the long-term safety of the structure and attracts the attention of relevant researchers (Wang, 1998). After extensive studies, it is now beyond doubt that fiber reinforcement

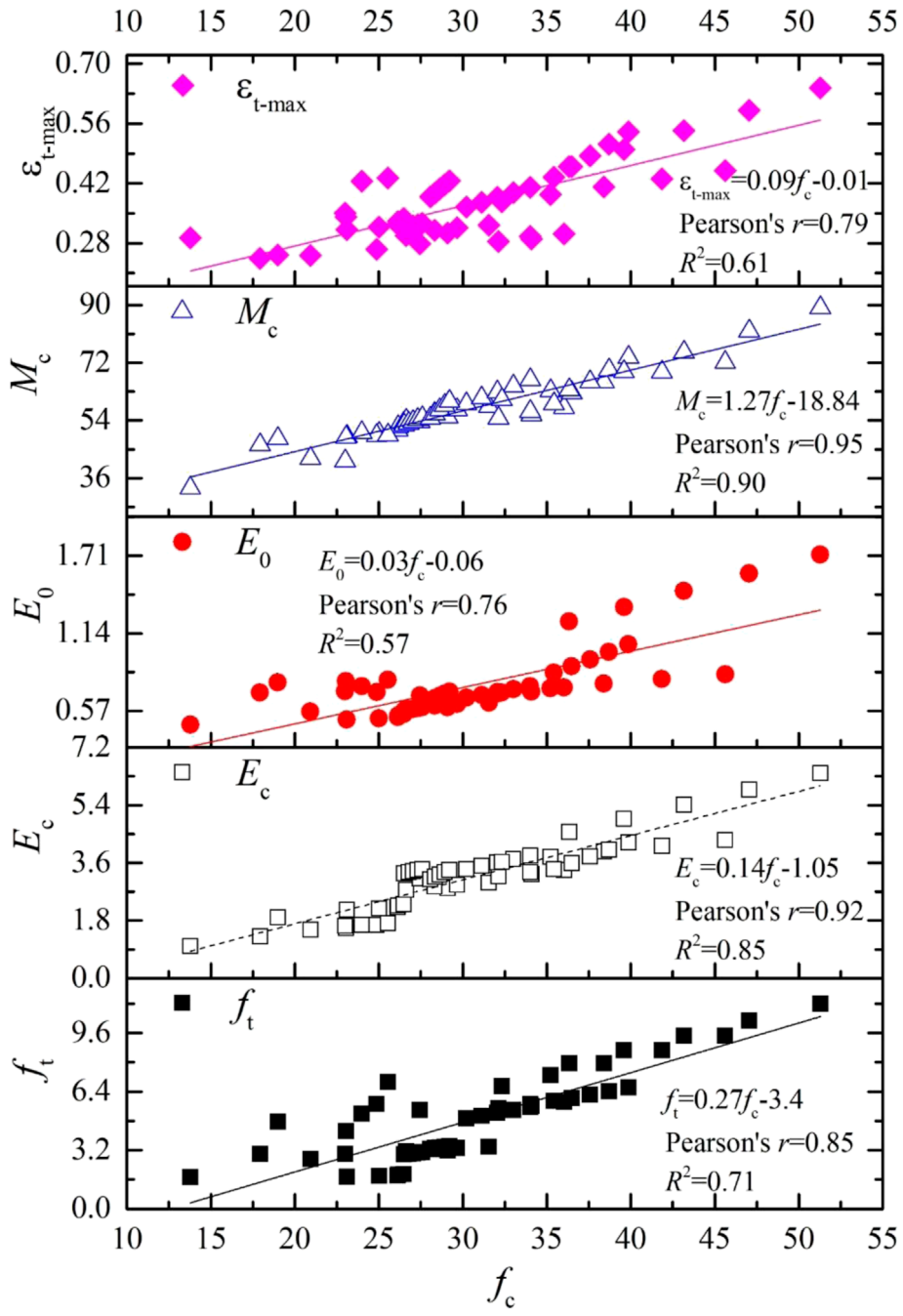

FIGURE 8
Correlations between compressive strength f_c, tensile strength f_t, Young's modulus E_c, elastic modulus E_0, total adsorbed energy M_c, and failure tensile strain $\varepsilon_{t\text{-}max}$.

can significantly improve the tensile properties of concrete. Orders of magnitude increases in toughness (energy absorption) over plain concrete were also commonly observed (Maiti et al., 2022; Wang et al., 2022; Zheng et al., 2022; Alarifi, 2023). Nonetheless, the long-term development of toughness considering the coupling effects of MK and SF was not reported until now.

As shown in Figure 7A, the toughness index M_c of MK-SF concrete (w/b = 0.6), with a total area of compressive strain-stress curve containing the pre-peak and post-peak region, developed with curing time. For SF = 0%, M_c of normal cement improved from 33.0 MPa to 53.1 MPa during 7–360 days. With MK adding, M_c of MK10-SF0 and MK15-SF0 were 46.4–58.5 MPa and 48.3–58.0 MPa. Results reveal that MK incorporation led to an increase in energy absorption and an ability to undergo larger plastic deformation. The presence of defects is considered an intrinsic cause of poor toughness in concrete. These defects lead to local tensile stresses

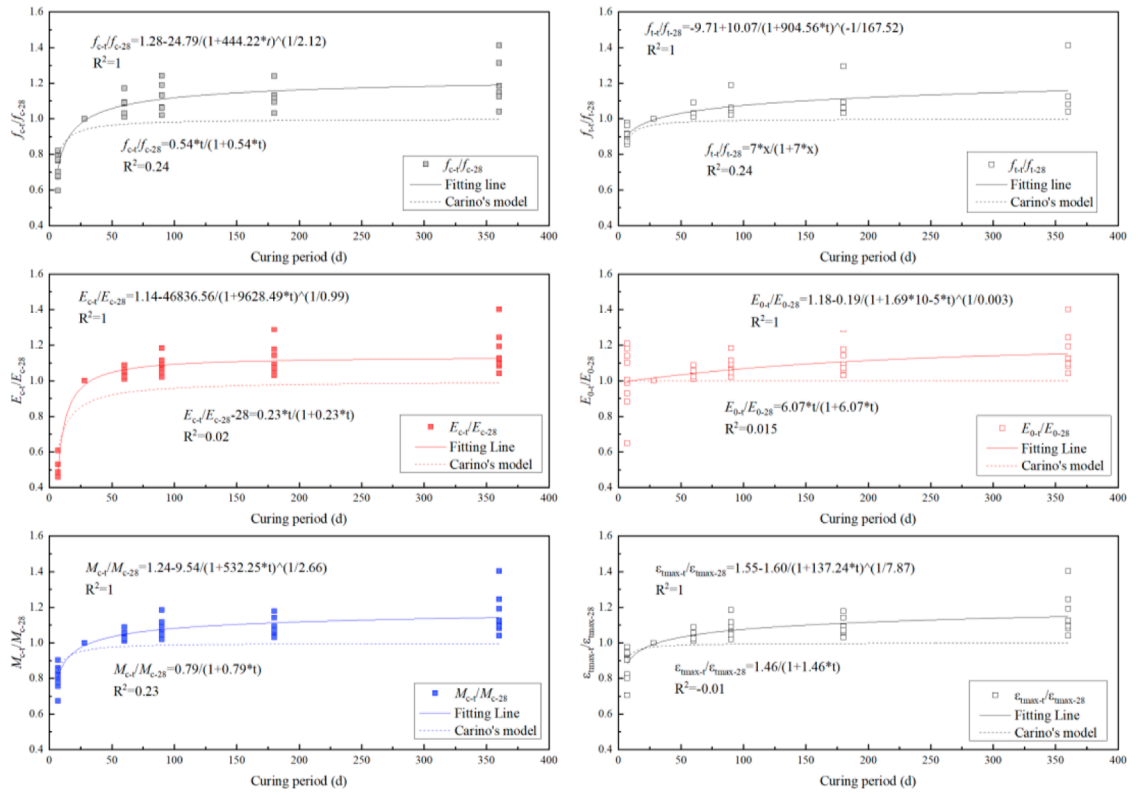

FIGURE 9
Prediction of compressive strength f_c, tensile strength f_t, Young's modulus E_c, elastic modulus E_0, total adsorbed energy M_c, and failure tensile strain $\varepsilon_{t\text{-}max}$ varying with curing age.

and stress concentrations, ultimately contributing to failure on a microscopic scale. Incorporating MK in concrete could help improve its toughness by reducing the size and amount of these defects. With SF addition, the influences of MK on M_c are more significant with curing time elapsed. For example, after 360 days of curing, the toughness values (M_c) of MK15-SF2 and MK15-SF3 were 1.24 and 1.54 times higher than those of MK15-SF0. At the early stages of curing, the toughness values of MK15-SF0, MK15-SF2, and MK15-SF3 were relatively similar. This suggests that the coupled effects of MK and SF on total energy absorption may not be significant in the early stages of curing. Additionally, it indicates that MK had a more dominant role in influencing toughness during the early stages, as observed in the SF = 0% group.

In Figure 7B, the tensile strain at peak stress ($\varepsilon_{t\text{-}max}$) of MK-SF concrete samples (with a water/binder ratio of 0.6) cured for different periods is shown. This parameter represents the ductility of concrete under tensile stress. The results indicate that the addition of MK alone has a limited impact on increasing $\varepsilon_{t\text{-}max}$, especially without the presence of SF. At the early stages of curing, the $\varepsilon_{t\text{-}max}$ values for MK0-SF0, MK10-SF0, and MK15-SF0 were 0.293, 0.245, and 0.298% respectively. As time passed, these values increased to 0.338, 0.323, and 0.302% after 360 days of curing. When SF is added at a concentration of 2%, 10%, and 15% MK promoted an increase in $\varepsilon_{t\text{-}max}$ of MK0-SF2 by 1.36 and 1.50 times respectively after 7 days of curing. After 360 days, the $\varepsilon_{t\text{-}max}$ values of MK0-SF2, MK10-SF2, and MK15-SF2 were 0.327, 0.411, and 0.459% respectively. Similarly, with an SF concentration of 3%, 10%, and 15% MK promoted an increase in $\varepsilon_{t\text{-}max}$ of MK0-SF3 by 1.20 and 1.12 fold respectively at the early stage. After long-term curing, the $\varepsilon_{t\text{-}max}$ values of MK0-SF3, MK10-SF3, and MK15-SF3 were 0.426, 0.541, and 0.643% respectively. These findings confirm that the addition of SF improves the ductility of concrete. Additionally, MK enhances the hydration degree and significantly increases the long-term ductility of SF-reinforced concrete. Without the presence of SF, MK has little contribution to ductility, and the brittleness of the concrete remains almost unchanged.

4.2 Prediction of long-term mechanical performance

In Figure 8, regression analysis on the correlation between several strength and ductility parameters of MK-SF concrete (w/b = 0.6), which are compressive strength f_c, tensile strength f_t, Young's modulus E_c, elastic modulus E_0, total absorb energy M_c and tensile strain at peak stress $\varepsilon_{t\text{-}max}$, are presented. The results indicate that the long-term relationships between f_c-f_t, f_c-E_c, f_c-E_0, f_c-M_c, and f_c-$\varepsilon_{t\text{-}max}$ of MK-modified fiber-reinforced concrete were suitably described by linear equations. The Pearson correlation coefficient r and the goodness of fit R^2 are commonly employed to assess the linear correlation between two variables, X and Y, as well as the degree of fitting of the regression line to the observed data. The

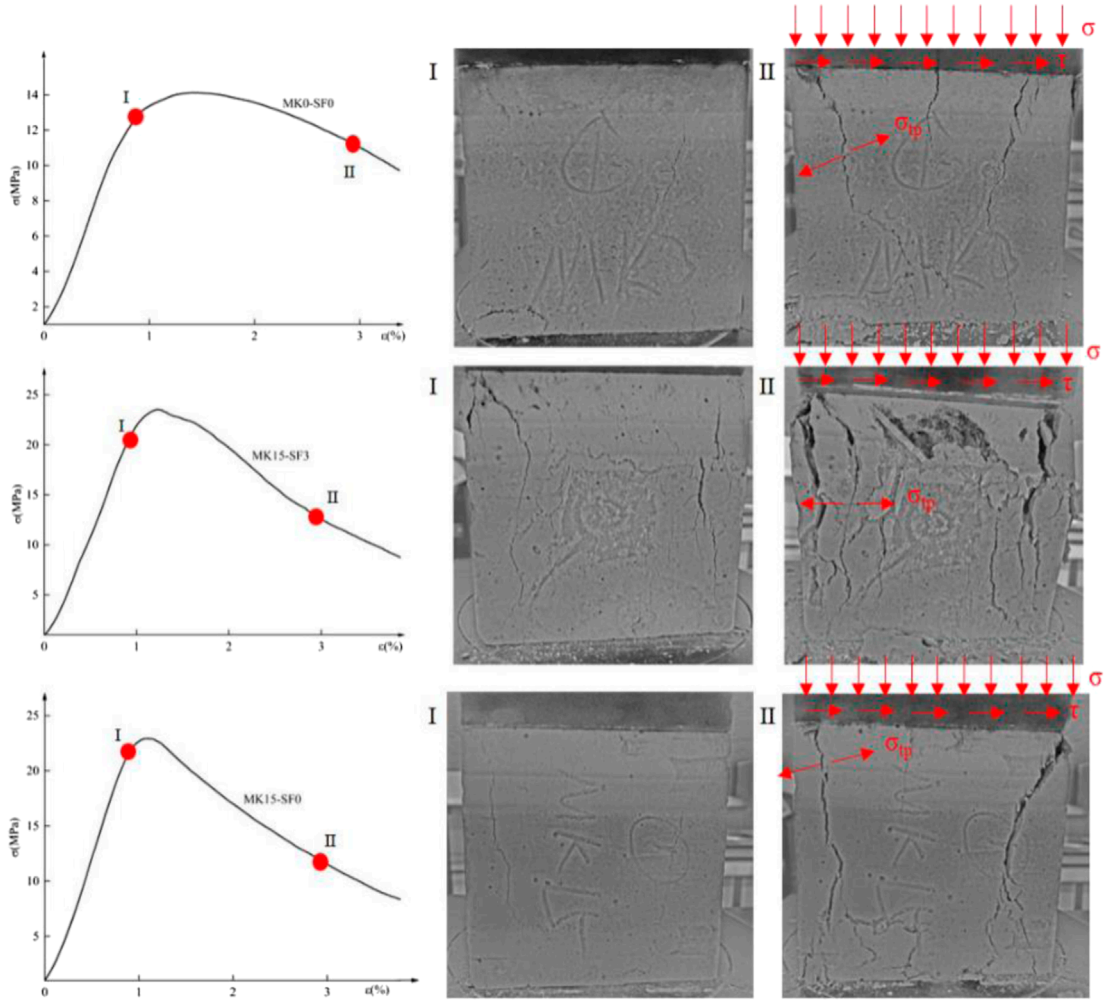

FIGURE 10
Crack development of specimen MK0-SF0, MK15-SF3, and MK15-SF0 under compression.

equations for these two indices are expressed as follows:

$$r = \frac{\sum_{i=1}^{n}\left(X_i-\overline{X}\right)\left(Y_i-\overline{Y}\right)}{\sqrt{\sum_{i=1}^{n}\left(X_i-\overline{X}\right)^2}\sqrt{\sum_{i=1}^{n}\left(Y_i-\overline{Y}\right)^2}} \tag{3}$$

$$R^2 = \frac{\left|\sum_{i=1}^{n}\left(X_i-\overline{X}\right)\left(Y_i-\overline{Y}\right)\right|^2}{\sum_{i=1}^{n}\left(X_i-\overline{X}\right)^2\sum_{i=1}^{n}\left(Y_i-\overline{Y}\right)^2} \tag{4}$$

Where X_i is the independent variable, Y_i is the dependent variable, $\overline{X}$ and $\overline{Y}$ are mean values. The Pearson correlation coefficient r of long-term f_c-f_t, f_c-E_c, f_c-E_0, f_c-M_c, and f_c-$\varepsilon_{t\text{-}max}$ relationships are 0.85, 0.92, 0.76, 0.95, and 0.79 respectively, indicating extreme (0.8–1.0) or strong relevant (0.6–0.8) of them with varying curing time. Their goodness of fit R^2 are 0.71, 0.85, 0.57, 0.90, and 0.61, revealing a good fitting result by linear equation regarding different curing periods.

Over the past several decades, many researchers have investigated the combined influence of time and curing temperature on the compressive strength development of concrete (Yi et al., 2005). Various relationship equations between curing condition and strength, such as the logarithmic model and the parabolic model have been suggested (Liao et al., 2008). Tank and Carino proposed a rate constant model being determined simultaneously from regression analyses on experimental data of concrete strength (Tank and Carino, 1991). However, existing models were normally applied to ages less than 28 days and are not applicable for ages greater than 28 days (Guo, 1990; Kjellsen and Detwiler, 1993; Kim et al., 1998). Among them, the widely used Carino's model showed that the development of strength can be described by a hyperbolic expression:

$$f = \frac{f_u k_T t}{1 + k_T t} \tag{5}$$

Where f is compressive or tensile strength at curing age t, k_T is the initial slope of the relative strength (f/f_u) versus the t curve at temperature T, and f_u is the ultimate strength.

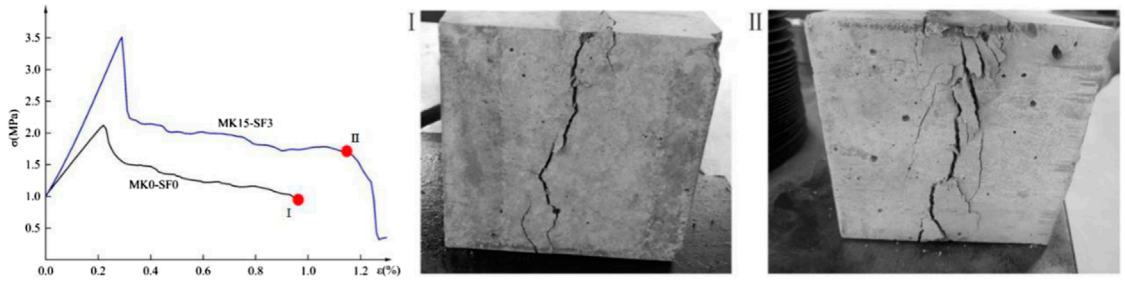

FIGURE 11
Images of tensile cracks under split tension.

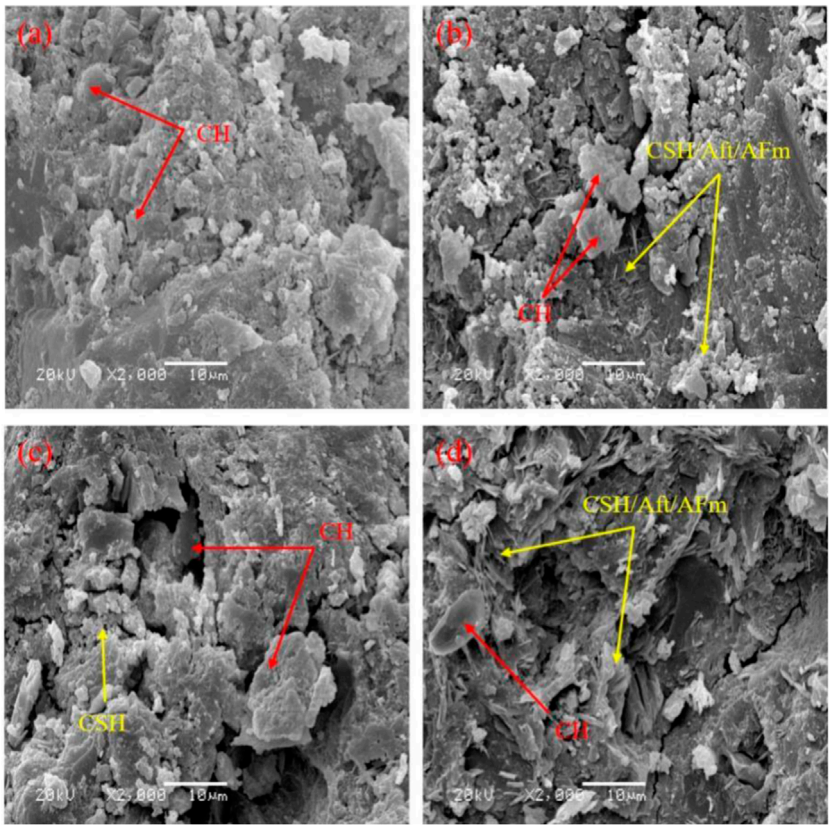

FIGURE 12
SEM images (magnified 2,000 times) of samples: **(A)** MK0-SF0; **(B)** MK15-SF0; **(C)** MK0-SF3; **(D)** MK15-SF3.

On the basis of a lack of an existing model, this paper proposes a new generalized hyperbola function to describe the long-term development of strength, deformation modulus, and toughness of MK-modified fiber-reinforced concrete. Firstly, a relative strength or toughness index $\lambda = f_c/f_{c\text{-}28}, f_t/f_{t\text{-}28}, E_c/E_{c\text{-}28}, E_0/E_{0\text{-}28}, M_c/M_{c\text{-}28,}$ and $\varepsilon_{tmax}/\varepsilon_{tmax\text{-}28}$ is used to replace strength at curing age. Secondly, a new generalized hyperbola function is used to fit experimental data:

$$\lambda = \left(a - \frac{b}{1+ct}\right)^{1/d} \tag{6}$$

Where a, b, c, and d are fitting parameters dependent on curing temperature and concrete composite, and t is curing age. Results in Figure 9 show the prediction of λ varying with curing age using Eq. 6 and Carino's model (Eq. 5). The goodness of fit R^2 using Eq. 6 is 1.0, and R^2 using Eq. 5 located in a lower level. It reveals that the generalized hyperbola function could effectively predict the long-term strength, deformation modulus, and toughness of MK-SF concrete.

4.3 Crack development

In Figure 10, the images of cracking development in the compression stage after 360 days of curing are shown for MK0-SF0,

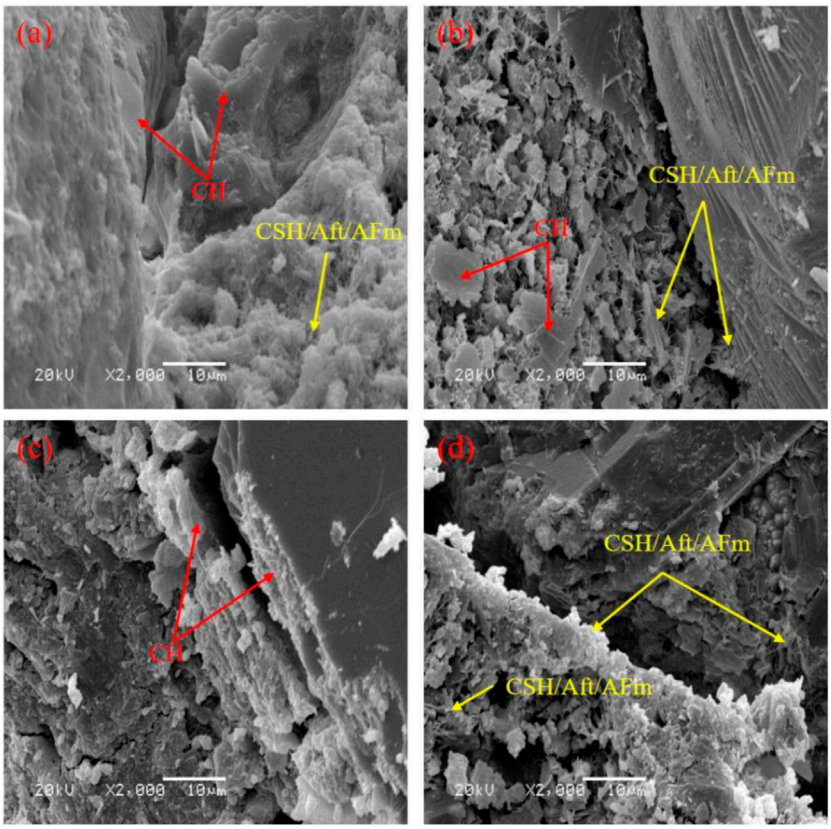

FIGURE 13
SEM images (magnified 2,000 times) of cracks between cementations and aggregates: **(A)** MK0-SF0; **(B)** MK15-SF0; **(C)** MK0-SF3; **(D)** MK15-SF3.

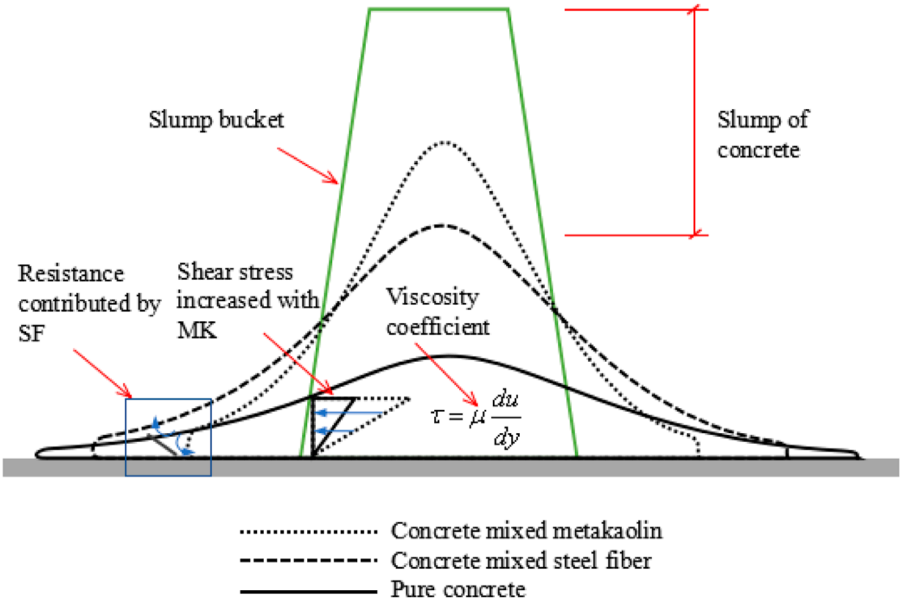

FIGURE 14
Schematic diagram of SF and MK influences on fluidness of concretes.

10.3389/fmats.2023.1162053

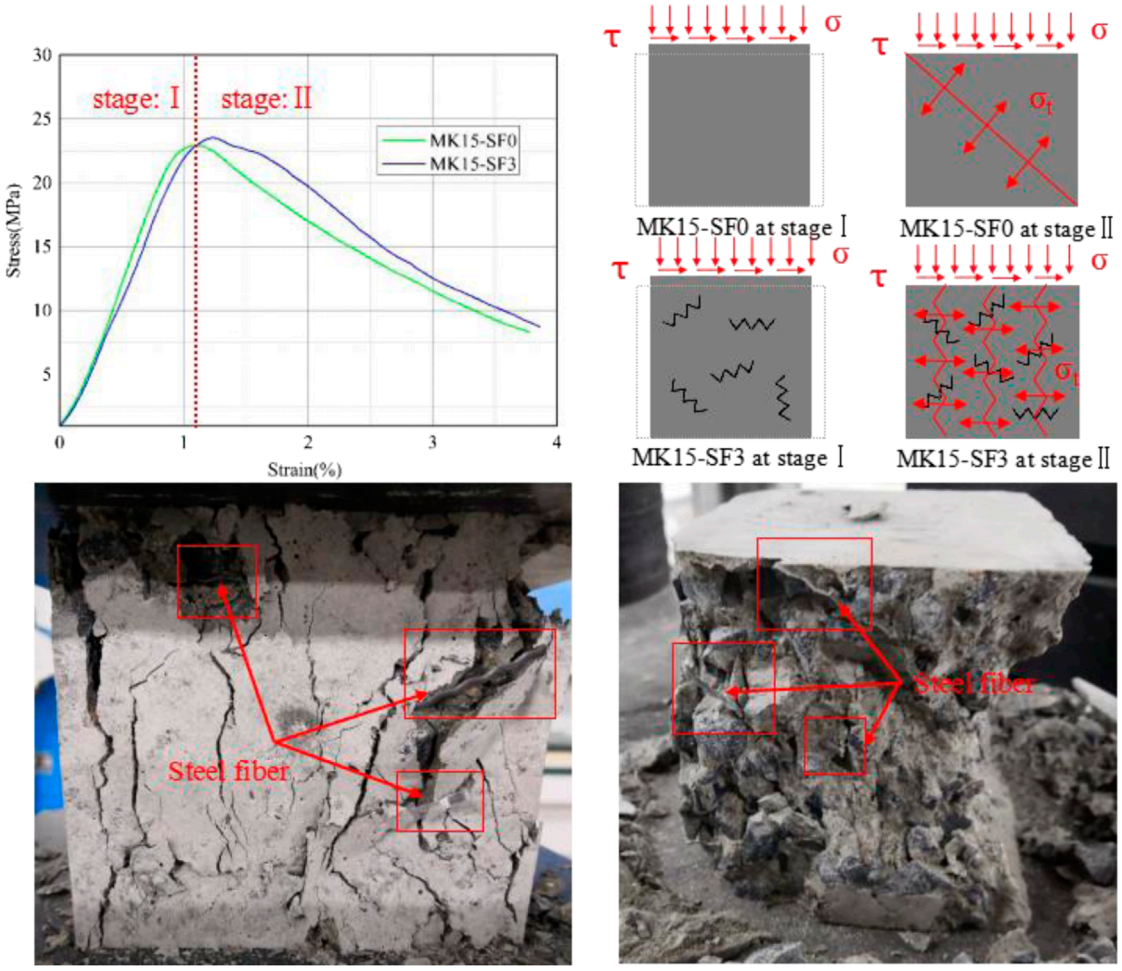

FIGURE 15
Schematic diagram of SF and MK influences on compression behavior of concretes.

MK15-SF3, and MK15-SF0 concrete samples (with a water/binder ratio of 0.6). For MK0-SF0, the angles between the crack surface and the vertical face are close to 45°, indicating a traditional failure mode for concrete under compression. However, for MK15-SF3, the angles between the crack and the vertical face after destruction are almost 90°, which is different from the traditional failure mode. The results suggest that the addition of SF significantly changed the direction of the main tensile forces in the concrete. In MK-SF concrete, SF had a dominant influence on the direction of cracks during the compression process, and the replacement rate of MK affected the critical tensile stress at crack initiation.

In Figure 11, the images of MK0-SF0 and MK15-SF3 concrete samples (w/b = 0.6) after tensile failure are shown. MK0-SF0 showed a continuous main crack connecting two contact points, whereas MK15-SF3 exhibited many diagonal cracks developed from the main crack connecting two loading points. By comparing the crack morphology of these samples, the inclusion of SF significantly alters the crack development and failure behavior of the concrete, leading to a more ductile mode of failure compared to the traditional brittle failure mode seen in plain concrete.

4.4 Microstructures

In Figure 12, SEM images of MK-SF concrete (with a water/binder ratio of 0.6) after 360 days of curing are shown (magnified 2,000 times). For MK0-SF0 and MK0-SF3 samples (Figures 12A, C), the particles are larger, and there are more defects such as cracks and pores present. It can be observed that SF has no significant influence on the microstructure of the MK-SF concrete. However, for samples partially replaced by MK, the geometry of the products becomes more complex, and the inter-particle defects are reduced. Additionally, the replacement of cement with MK promotes the conversion of Calcium Hydroxide (CH) to Hydrated Calcium Silicate (CSH), and the adhesion between CSH and the aggregate becomes stronger. More CSH products can be observed in MK15-SF0 and MK15-SF3 samples (Figures 12B, D), indicating an increased strength of inter-particle binding.

Figure 13 depicts SEM images of the interfacial transition zone (ITZ) between the aggregate and matrix of MK0-SF0, MK15-SF0, MK0-SF3, and MK15-SF3 (with a water/binder ratio of 0.6) after 360 days of curing. In both Figures 13A, C, the bonding between the aggregates and the products in the ITZ is observed to be

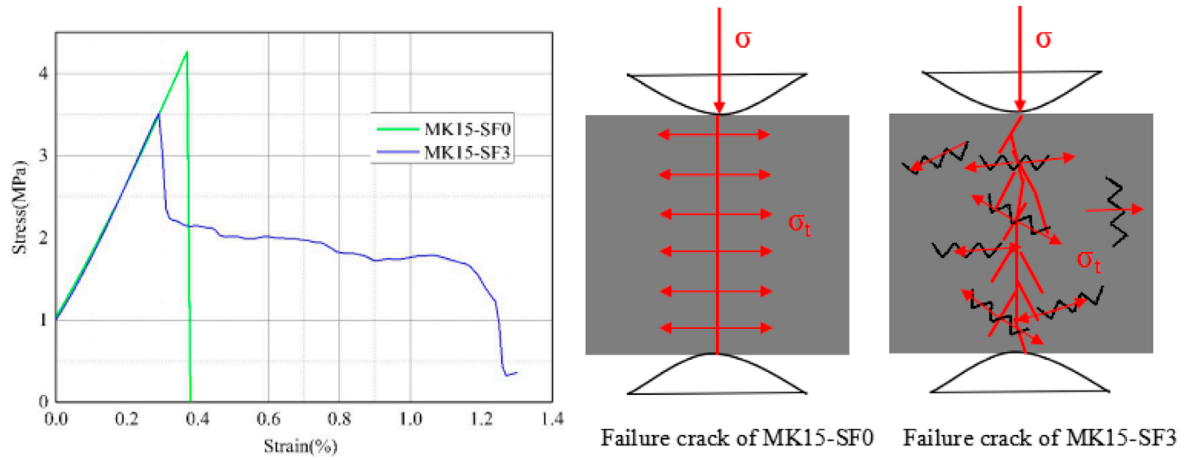

FIGURE 16
Schematic diagram of SF and MK influences on tension behavior of concretes.

broken, regardless of the presence of MK. The ITZ region contains a higher amount of Calcium Hydroxide (CH) products in the form of hexagonal plates, and fewer Hydrated Calcium Silicate (CSH) products in the form of acicular and fibrous particles. This implies that the bonding between the aggregate and products is weak due to the predominantly weaker bonding consisting of CH products. However, in Figures 13B, D, a significant amount of CSH cementation is bonded with the aggregates when MK is added. This enhanced bonding strength within the interfacial transition zone (ITZ) is a result of the increased presence of CSH products, due to the addition of MK.

4.5 Mechanisms

The mechanisms of the above results can be summarized as below:

Firstly, as shown in Figure 14, the finer MK powder with a higher specific area adsorbs more water, and then it significantly reduces the fluidity of concrete at the mixing stage when the ratios of water to cementing material are uniform (Qin et al., 2019). When the SF are incorporated, a lateral resistance prevents the slurry from spreading around, and the disordered structure increases the friction between SF and slurry. As MK contents increase, the viscosity coefficient dominates the fluidity of mixtures, thus the coupling effects on the fluidness reducing are not evident. With lower w/b, influences of SF and MK addition on the reduction of fluidity are more profound.

Secondly, previous studies proposed that a large amount of unstable calcium hydroxide (CH) was produced during the pozzolanic reaction in cement, and the activated aluminate and activated silicate in MK consumed the unstable Calcium Hydroxide (CH) in the slurry to form a more stable Hydrated Calcium Silicate (CSH) gel, Hydrated calcium aluminate (C_3AH_6), and hydrated calcium sulfoaluminate (C_2ASH_8) (Poon et al., 2006; Siddique and Klaus, 2009; Güneyisi et al., 2010; Melo and Carneiro, 2010; Kou et al., 2011; Megat Johari et al., 2011; Antoni et al., 2012; Bernal et al., 2012; Güneyisi et al., 2012; Madandoust and Mousavi, 2012; Ramezanianpour and Bahrami Jovein, 2012; Duan et al., 2013; Rashad, 2013; Han et al., 2018). Meanwhile, the calcium carbonate $CaCO_3$ reacting with activated alumina in MK forms supplementary AFm phase matters such as ettringite (Güneyisi et al., 2010; Antoni et al., 2012; Bernal et al., 2012; Güneyisi et al., 2012; Duan et al., 2013; Han et al., 2018). Based on SEM images, these products reduce the porosity and defects and strengthen the inter-particle bonding. As a result, the compressive strength, splitting tensile strength, Young's and elastic modulus, the total absorbed energy and tensile strain at peak stress of MK-treated concrete are improved (Zhang et al., 2015).

Thirdly, the steel fibers restricted the slippage of aggregates and cementations during the deformation or cracking in the sample (Qiana and Stroeven, 2000; Yao et al., 2003; Song and Hwang, 2004; Yazıcı et al., 2007; Mohammadi et al., 2008; Holschemacher et al., 2010). Notably, the SF does not react with the cementing components in the concrete. Instead, SF provides a physical constraint on the concrete by exerting friction on the interfacial transition zone. As shown in Figure 15, the cohesion forces between different composites, contributed by MK and cement, control the deformation in the pre-cracking stage. When cracks and plastic strain develop, the presence of steel fibers changes the direction of the main tensile stresses. Additionally, the strong bonding between the cementations and steel fibers, resulting from the higher degree of hydration reaction with MK incorporation and increasing curing age, significantly improves the coupling effects of MK and SF on strength and toughness. In Figure 16, it can be observed that in concrete without SF, the failure mode is bristle-shaped. However, the inclusion of steel fibers constrains surface separation and contributes to residual strength after crack development. The presence of SF also influences the direction of the main crack and main tensile forces. Moreover, the strong bonding between SF and the matrix at the interfacial transition zone increases the maximum tension stress. As a result, MK plays a dominant role in enhancing long-term strength, deformation modulus, and toughness. Meanwhile, SF affects the direction of the main tensile forces in the concrete and influences the morphology of cracks in compression and tension processes.

5 Conclusion

In this paper, the long-term mechanical performance of Metakaolin-Steel Fiber (MK-SF) concrete in high fluidity state, including compressive strength, tensile strength, Young's modulus, elastic modulus, total absorbed energy until failure, and tensile strain at peak stress, were comprehensively investigated. A new generalized hyperbola was proposed to predict the above long-term mechanical behavior. Based on crack morphology and microstructure analysis, the mechanism of coupling effects of MK and steel fiber on this unusual high fluidity concrete were summarized. Then, several conclusions are drawn as follows:

1. The slump of fresh concrete decreased with increasing MK replacement rates or SF content with different ratios of water to binders. MK-treated concrete admixed with a w/b ratio 0.6 showed a very high slump of 160–200 mm. With decreasing w/b ratio, the slump decreased to nearly 100 mm. The coupling effects of SF and MK on the fluidness were not significant when MK content was higher.
2. After different curing ages, the compressive and tensile strength of high fluidity MK-SF concrete (w/b = 0.6) increased with the increase of MK and SF replacement rate. The effect of MK and SF coupling on the compressive strength f_c is more evident after long-term curing. Tensile strength f_t of MK15-SF3 increases from 6.9 to 11.2 MPa during 7–360 days of curing, while MK0-SF3 is 2.99–3.41 MPa varying with curing period. Without MK incorporation, the effect of SF and curing time on f_t is not significant.
3. At the pre-peak stress region of the compressive and tensile strain-stress curve, Young's modulus E_c, elastic modulus $E_{0,}$ and tensile strain at peak stress $\varepsilon_{t\text{-}max}$ increased significantly with the increase of MK and SF replacement rates with different curing ages. The coupling effects of MK and SF are more prominent after long-term curing. At the post-peak stress region of compressive and tensile strain-stress curves, there exists a residual stage. The residual strengths are improved by MK.
4. The toughness index M_c, the total area of compressive strain-stress curve containing pre-peak and post-peak region, develops with curing time and MK and SF admixture amount. With SF addition, the influence of MK on M_c is more significant with curing time elapsed. For example, after 360 days of curing, M_c of MK15-SF2 and MK15-SF3 are 1.24 and 1.54 times than MK15-SF0. At the early stage, the M_c of MK15-SF0, MK15-SF2, and MK15-SF3 are close.
5. Regression analysis explores that a linear equation commendably describes long-term f_c-f_t, f_c-E_c, f_c-E_0, f_c-M_c and f_c-$\varepsilon_{t\text{-}max}$ relationships of MK-modified fiber-reinforced concrete. Their Pearson correlation coefficients (*r)* are 0.85, 0.92, 0.76, 0.95, and 0.79 respectively, indicating extreme (0.8–1.0) or strong relevence (0.6–0.8) with varying curing time. Their goodness of fits R^2 are 0.71, 0.85, 0.57, 0.90, and 0.61, revealing a good fitting result by a linear equation. A relative strength or toughness index λ and a new generalized hyperbola function are proposed to predict the long-term mechanical behavior of MK-SF concrete.
6. The angle between the crack and vertical face of concrete containing SF is about 90° after destruction under compression, while that of MK15-SF0 is 45° which is close to MK0-SF0. The results indicate that SF dominates the direction of crack and main tensile forces in compression processes. In the tension process, the MK0-SF0 destructs along a continuous main crack connecting two contact points, and there exist many diagonal cracks developed from the main crack connecting two loading points in MK15-SF3.
7. Based on microstructure observation, more stable Hydrated Calcium Silicate (CSH) gel and AFm phase matters are produced during long-term second pozzolanic reaction activated by MK. These products reduce the porosity and defects and strengthen the bonding in the interfacial transition zone.

Data availability statement

The original contributions presented in the study are included in the article/supplementary material, further inquiries can be directed to the corresponding author.

Author contributions

HD contributed to conception and design of the study. HD organized the database. HX performed the statistical analysis. HD wrote the first draft of the manuscript. JX wrote sections of the manuscript. All authors contributed to the article and approved the submitted version.

Funding

The authors declare that this study received funding from Gansu Road and Bridge Construction Group Co., Ltd. The funder was not involved in the study design, collection, analysis, interpretation of data, the writing of this article, or the decision to submit it for publication.

Conflict of interest

HX, JX were employed by Gansu Road and Bridge Construction Group Co., Ltd.

The remaining authors declare that the research was conducted in the absence of any commercial or financial relationships that could be construed as a potential conflict of interest.

Publisher's note

References

Akcay, B., and Tasdemir, M. A. (2018). Performance evaluation of silica fume and metakaolin with identical finenesses in self compacting and fiber reinforced concretes. *Constr. Build. Mater.* 185, 436–444. doi:10.1016/j.conbuildmat.2018.07.061

Alarifi, I. M. (2023). A review on factors affecting machinability and properties of fiber-reinforced polymer composites. *J. Nat. Fibers* 20 (1), 20. doi:10.1080/15440478.2022.2154304

Albidah, A., Altheeb, A., Alrshoudi, F., Abadel, A., Abbas, H., and Al-Salloum, Y. (2020). Bond performance of GFRP and steel rebars embedded in metakaolin based geopolymer concrete. *Structures* 27, 1582–1593. doi:10.1016/j.istruc.2020.07.048

Antoni, M., Rossen, J., Martirena, F., and Scrivener, K. (2012). Cement substitution by a combination of metakaolin and limestone. *Cem. Concr. Res.* 42 (12), 1579–1589. doi:10.1016/j.cemconres.2012.09.006

Bernal, S. A., Mejía de Gutiérrez, R., and Provis, J. L. (2012). Engineering and durability properties of concretes based on alkali-activated granulated blast furnace slag/metakaolin blends. *Constr. Build. Mater.* 33, 99–108. doi:10.1016/j.conbuildmat.2012.01.017

Del Savio, A. A., Esquivel, D. L., Carrillo, J., and Yep, E. C. (2022). Determination of polypropylene fiber-reinforced concrete compressive strength and elasticity modulus via ultrasonic pulse tests. *Appl. Sci-Basel* 12 (20), 10375. doi:10.3390/app122010375

Duan, P., Shui, Z., Chen, W., and Shen, C. (2013). Effects of metakaolin, silica fume and slag on pore structure, interfacial transition zone and compressive strength of concrete. *Constr. Build. Mater.* 44, 1–6. doi:10.1016/j.conbuildmat.2013.02.075

Güneyisi, E., Gesoğlu, M., Akoi, A. O. M., and Mermerdaş, K. (2014). Combined effect of steel fiber and metakaolin incorporation on mechanical properties of concrete. *Compos. Part B Eng.* 56, 83–91. doi:10.1016/j.compositesb.2013.08.002

Güneyisi, E., Gesoğlu, M., Karaoğlu, S., and Mermerdaş, K. (2012). Strength, permeability and shrinkage cracking of silica fume and metakaolin concretes. *Constr. Build. Mater.* 34, 120–130. doi:10.1016/j.conbuildmat.2012.02.017

Güneyisi, E., Gesoğlu, M., and Özbay, E. (2010). Strength and drying shrinkage properties of self-compacting concretes incorporating multi-system blended mineral admixtures. *Constr. Build. Mater.* 24 (10), 1878–1887. doi:10.1016/j.conbuildmat.2010.04.015

Guo, C. G. (1990). Maturity of concrete - method for predicting early-stage strength - closure. *Aci Mater J.* 87 (3), 298–299.

Han, J., Shui, Z., Wang, G., Sun, T., and Gao, X. (2018). Performance evaluation of steam cured HPC pipe piles produced with metakaolin based mineral additives. *Constr. Build. Mater.* 189, 719–727. doi:10.1016/j.conbuildmat.2018.09.044

Holschemacher, K., Mueller, T., and Ribakov, Y. (2010). Effect of steel fibres on mechanical properties of high-strength concrete. *Mater. Des.* 31 (5), 2604–2615. doi:10.1016/j.matdes.2009.11.025

Kim, J. K., Moon, Y. H., and Eo, S. H. (1998). Compressive strength development of concrete with different curing time and temperature. *Cem. Concr. Res.* 28 (12), 1761–1773. doi:10.1016/s0008-8846(98)00164-1

Kim, W., Jeong, K., Choi, H., and Lee, T. (2022). Correlation analysis of ultrasonic pulse velocity and mechanical properties of normal aggregate and lightweight aggregate concretes in 30-60 MPa range. *Materials* 15 (8), 2952. doi:10.3390/ma15082952

Kjellsen, K. O., and Detwiler, R. J. (1993). Later-age strength prediction by a modified maturity model. *Aci Mater J.* 90 (3), 220–227.

Kou, S. C., Poon, C. S., and Agrela, F. (2011). Comparisons of natural and recycled aggregate concretes prepared with the addition of different mineral admixtures. *Cem. Concr. Compos.* 33 (8), 788–795. doi:10.1016/j.cemconcomp.2011.05.009

Li, J., Hong, J., Liu, S. Y., Zhou, Y. Z., and Meng, K. (2023). Multiaxial compressive strength of hybrid fiber reinforced concrete: A unified empirical model. *Front. Mater* 10, 10. doi:10.3389/fmats.2023.1100868

Liao, W. C., Lee, B. J., and Kang, C. W. (2008). A humidity-adjusted maturity function for the early age strength prediction of concrete. *Cem. Concr. Comp.* 30 (6), 515–523. doi:10.1016/j.cemconcomp.2008.02.006

Madandoust, R., and Mousavi, S. Y. (2012). Fresh and hardened properties of self-compacting concrete containing metakaolin. *Constr. Build. Mater.* 35, 752–760. doi:10.1016/j.conbuildmat.2012.04.109

Mahapatra, C. K., and Barai, S. V. (2019). Sustainable self compacting hybrid fiber reinforced concrete using waste materials. *Struct. Concr.* 20 (2), 756–765. doi:10.1002/suco.201700239

Maiti, S., Islam, M. R., Uddin, M. A., Afroj, S., Eichhorn, S. J., and Karim, N. (2022). Sustainable fiber-reinforced composites: A review. *Adv. Sustain Syst.* 6 (11), 2200258. doi:10.1002/adsu.202200258

Megat Johari, M. A., Brooks, J. J., Kabir, S., and Rivard, P. (2011). Influence of supplementary cementitious materials on engineering properties of high strength concrete. *Constr. Build. Mater.* 25 (5), 2639–2648. doi:10.1016/j.conbuildmat.2010.12.013

Mehdipour, S., Nikbin, I. M., Dezhampanah, S., Mohebbi, R., Moghadam, H., Charkhtab, S., et al. (2020). Mechanical properties, durability and environmental evaluation of rubberized concrete incorporating steel fiber and metakaolin at elevated temperatures. *J. Clean. Prod.* 254, 120126. doi:10.1016/j.jclepro.2020.120126

Melo, K. A., and Carneiro, A. M. P. (2010). Effect of Metakaolin's finesses and content in self-consolidating concrete. *Constr. Build. Mater.* 24 (8), 1529–1535. doi:10.1016/j.conbuildmat.2010.02.002

Mohammadi, Y., Singh, S. P., and Kaushik, S. K. (2008). Properties of steel fibrous concrete containing mixed fibres in fresh and hardened state. *Constr. Build. Mater.* 22 (5), 956–965. doi:10.1016/j.conbuildmat.2006.12.004

Mohammed, A. A., Ahmed, H. U., and Mosavi, A. (2021). Survey of mechanical properties of geopolymer concrete: A comprehensive review and data analysis. *Materials* 14 (16), 4690. doi:10.3390/ma14164690

Noroozi, R., Shafabakhsh, G., Kheyroddin, A., and Moghaddam, A. M. (2019). Investigating the effects of recycled PET particles, shredded recycled steel fibers and Metakaolin powder on the properties of RCCP. *Constr. Build. Mater* 224, 173–187. doi:10.1016/j.conbuildmat.2019.07.012

Poon, C. S., Kou, S. C., and Lam, L. (2006). Compressive strength, chloride diffusivity and pore structure of high performance metakaolin and silica fume concrete. *Constr. Build. Mater.* 20 (10), 858–865. doi:10.1016/j.conbuildmat.2005.07.001

Qiana, C. X., and Stroeven, P. (2000). Development of hybrid polypropylene-steel fibre-reinforced concrete. *Cem. Concr. Res.* 30, 63–69. doi:10.1016/s0008-8846(99)00202-1

Qin, Z., Zhou, S., Ma, C., Long, G., Xie, Y., and Chen, B. (2019). Roles of metakaolin in magnesium phosphate cement: Effect of the replacement ratio of magnesia by metakaolin with different particle sizes. *Constr. Build. Mater.* 227, 116675. doi:10.1016/j.conbuildmat.2019.116675

Ramezanianpour, A. A., and Bahrami Jovein, H. (2012). Influence of metakaolin as supplementary cementing material on strength and durability of concretes. *Constr. Build. Mater.* 30, 470–479. doi:10.1016/j.conbuildmat.2011.12.050

Rashad, A. M. (2013). Metakaolin as cementitious material: History, scours, production and composition – a comprehensive overview. *Constr. Build. Mater.* 41, 303–318. doi:10.1016/j.conbuildmat.2012.12.001

Shafigh, P., Nomeli, M. A., Alengaram, U. J., Bin Mahmud, H., and Jumaat, M. Z. (2016). Engineering properties of lightweight aggregate concrete containing limestone powder and high volume fly ash. *J. Clean. Prod.* 135, 148–157. doi:10.1016/j.jclepro.2016.06.082

Siddique, R., and Klaus, J. (2009). Influence of metakaolin on the properties of mortar and concrete: A review. *Appl. Clay Sci.* 43 (3-4), 392–400. doi:10.1016/j.clay.2008.11.007

Song, P. S., and Hwang, S. (2004). Mechanical properties of high-strength steel fiber-reinforced concrete. *Constr. Build. Mater.* 18 (9), 669–673. doi:10.1016/j.conbuildmat.2004.04.027

Tank, R. C., and Carino, N. J. (1991). Rate-constant functions for strength development of concrete. *Aci Mater J.* 88 (1), 74–83.

Wang, Y. (1998). Toughness characteristics of synthetic fibre-reinforced cementitious composites. *Fatigue Fract. Eng. M.* 21 (4), 521–532. doi:10.1046/j.1460-2695.1998.00045.x

Wang, Z. G., Fang, Z. Y., Xie, Z. Q., and Smith, D. E. (2022). A review on microstructural formations of discontinuous fiber-reinforced polymer composites prepared via material extrusion additive manufacturing: Fiber orientation, fiber attrition, and micro-voids distribution. *Polymers-Basel* 14 (22), 4941. doi:10.3390/polym14224941

Yao, W., Li, J., and Wu, K. (2003). Mechanical properties of hybrid fiber-reinforced concrete at low fiber volume fraction. *Cem. Concr. Res.* 33, 27–30. doi:10.1016/s0008-8846(02)00913-4

Yazıcı, Ş., İnan, G., and Tabak, V. (2007). Effect of aspect ratio and volume fraction of steel fiber on the mechanical properties of SFRC. *Constr. Build. Mater.* 21 (6), 1250–1253. doi:10.1016/j.conbuildmat.2006.05.025

Yi, S. T., Moon, Y. H., and Kim, J. K. (2005). Long-term strength prediction of concrete with curing temperature. *Cem. Concr. Res.* 35 (10), 1961–1969. doi:10.1016/j.cemconres.2005.06.010

Yu, Z. H., Zhang, T. W., and Deng, Y. F. (2022). The micro-facial characteristics and mechanical behavior of metakaolin and steel fibers modified concrete at high fluidity. *Case Stud. Constr. Mat.* 16, e01019. doi:10.1016/j.cscm.2022.e01019

Zhang, Q. Q., Xu, X., Li, H., Xiong, G. P., Hu, H., and Fisher, T. S. (2015). Mechanically robust honeycomb graphene aerogel multifunctional polymer composites. *Carbon* 93, 659–670. doi:10.1016/j.carbon.2015.05.102

Zheng, Y. X., Zhang, Y., Zhuo, J. B., Zhang, Y. M., and Wan, C. (2022). A review of the mechanical properties and durability of basalt fiber-reinforced concrete. *Constr. Build. Mater* 359, 129360. doi:10.1016/j.conbuildmat.2022.129360